15.3   PRESSURE MEASUREMENTS AT THE GROUND IN AN F-4 TORNADO

Julian J. Lee* and Timothy M. Samaras
Applied Research Associates Inc., Littleton, Colorado

Carl R. Young
Desert Research Institute / University of Nevada, Reno, Nevada

1.INTRODUCTION

Direct measurements of flow properties inside tornadoes have been accomplished in the past through remote Doppler radar instruments, fortuitous passages of tornadoes over stationary meteorological stations, and relatively rare deployments of specialized in-situ instrumentation. In addition to the transient and unpredictable nature of tornado occurrences, measurements using in-situ instruments are complicated by the challenge of placing instruments in the tornado path, not to mention survival and proper operation of the instruments in the harsh tornadic environment.

Many attempts to deploy in-situ instruments have been made with varying degrees of success (Samaras 2004). A few deployments are notable for the measurements made in close proximity to the tornado core. The instrumented probe called TOTO was deployed near an F-2 tornado, recording a maximum pressure drop of 5 mb (Bluestein and Golden 1993). A more compact probe was deployed 1.6 km from a tornado near Mooreland, OK, recording a peak pressure drop of 4 mb (Bluestein and Golden 1993). Several instrumented probes were deployed near an F-4 tornado west of Allison, TX, on June 8th, 1995, with the tornado axis passing within 660 m of one of the probes producing a peak pressure drop of 55 mb (Winn et. al. 1999). An aerodynamically-shaped instrumented probe called the HITPR (Hardened In-situ Tornado Pressure Recorder) was deployed near an F-3 tornado close to Pratt, KS on May 7th, 2002 recording a pressure drop of 24 mb (Samaras and Lee 2003). The HITPR features a very low-profile shape resulting in high stability in tornadic winds.

The HITPR was subsequently deployed inside the core of an F-0 tornado near Stratford, TX on May 15th, 2003, recording a peak pressure drop of about 40 mb. This tornado was being scanned remotely by Doppler radar instruments as the tornado passed over the probe, and a comparison of the remote and in-situ results is reported by Wurman and Samaras (2004). In-situ measurements are unquestionably extremely difficult to obtain, however they provide valuable insight into the morphology and flow dynamics within tornadoes.

In this paper, the results of a HITPR deployment in a tornado that passed through Manchester, SD, on June 24th, 2003 are reported. The synoptic and mesoscale conditions favorable to the tornado outbreak are described. The vortex flow features are then discussed through comparisons with analytical and laboratory-simulated models.

2.   INSTRUMENTATION

The HITPR probe used for the Manchester tornado measurements consists of a conical steel shell about 51 cm in diameter and 15 cm high containing instrumentation to measure pressure, temperature, humidity, and wind speed (Figure 1). The device also contains a data logger to record up to 2 hours of data onto a flash card. It is completely autonomous and weighs about 23 kg, facilitating rapid deployment in remote locations. The flow and atmospheric properties of the air on the surface of the device are recorded at a rate of 10 samples/second (10 Hz) through radially-located holes that communicate to the diagnostic gauges inside the shell. Details on the design and operation of the HITPR are given in Samaras and Lee 2003.

_____

*_Corresponding author address_: Julian J. Lee, Applied Research Associates Inc., 10720 Bradford Rd. Suite 110, Littleton, CO 80127; e-mail: jlee@ara.com

Figure 1. Picture of HITPR. Holes connecting to the diagnostic gauges inside the device are visible.

In order to survive the harsh environment inside a tornado, the HITPR shape was designed to have minimal aerodynamic forces in high winds. Thanks to its low profile, lift forces are small, and the probe can operate in winds up to 80 m/s.

3.   ENVIRONMENTAL CONDITIONS

On the morning of June 24, 2003, the synoptic pattern was conducive for a severe weather episode with supercells and tornadoes probable across the Northern Plains. High dewpoints and a deep moisture field, strong upper and mid level winds ahead of a progressive trough, convergence along a retreating warm front and outflow boundaries, and deep layer shear associated with backed surface flow and a veered wind profile operated in concert to provide the necessary ingredients for a significant tornadic outbreak. Favorable storm motion in the proximity of the frontal boundary and a cell merger helped produce the most violent tornado of the outbreak in Manchester, SD.
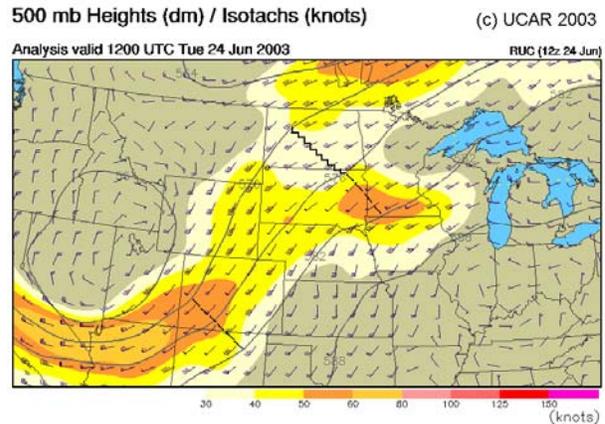

Figure 2. RUC upper air analysis shows the 1200 UTC 24 June 2003 500 mb heights (dm) and isotachs (in knots; 1 m s^{-1} equals .5144 knots). The dashed lines indicate the locations of short wave troughs and the sawtooth line denotes the shortwave ridge. [From UCAR 2003]

An analysis of the 1200 UTC (0700 central standard time) upper level charts on 24 June 2003, the 250 mb chart (not shown) indicated a strong trough centered over the Great Basin with a jet streak of 50+ m s^{-1} winds rounding its base. This trough was progged to progress northeastward during the day while ejecting upper and mid level jets into the Central and Northern Plains. Downstream of the progressive trough, a 500 mb short wave trough was migrating northeastward across central Minnesota and was associated with an ongoing elevated convective complex of storms across portions of the eastern Dakotas into the Great Lakes (Fig. 2). Numerous outflow boundaries were being produced and an extensive canopy of cirrus covered the region. The other midtropospheric short wave trough was moving northeastward across the Central Rockies and was expected to nose into the Northern Plains by late afternoon resulting in diffluent flow aloft, advection of steep lapse rates, and surface pressure falls ahead of the trough.

At 850 mb (not shown), a reasonably strong low level jet (LLJ) (southerly to southwesterly at 10-18 m s^{-1}) was advecting Gulf of Mexico moisture into the Northern Plains providing mixing ratios of 12-16 g kg^{-1} through eastern Nebraska. In response to pressure falls ahead of the approaching mid/upper level trough, the LLJ was expected to increase during the evening with southerly wind speeds of 20-25 m s^{-1} forecast across eastern NE, southeast SD, northwest IA, and southwest MN.
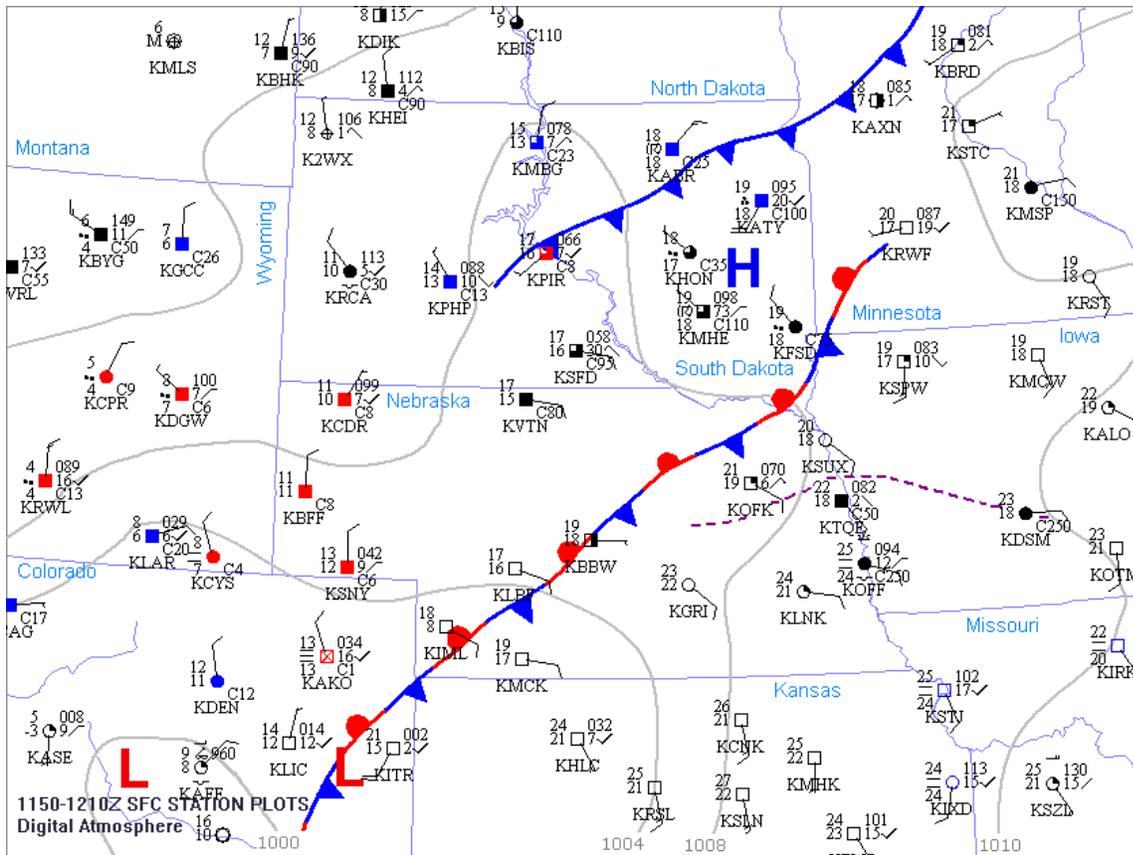
Figure 3. Surface analysis from 1200 UTC 24 June 2003 shows isobars (thin gray lines, contoured at 4 mb intervals) and location of frontal boundaries in Northern Plains. The frontal symbols are conventional with the dashed line denoting the stationary outflow boundary. The station plots display temperature and dewpoint readings in Celsius, sea level pressure (mb), 3-h pressure tendency, and winds in knots (1 m s^{-1} equals .5144 knots). [Analysis created using Weathergraphics Digital Atmosphere 2004]

At the surface at 1200 UTC (Fig. 3), a quasistationary frontal boundary extended from central MN southwestward through extreme southeast SD and southwest NE to a low pressure center in eastern CO, resulting in a southeasterly wind flow of 2-5 m s^{-1} across most of eastern NE. Due to reinforcement from the ongoing convection and a weak cross frontal wind field, the front would be expected to drift slowly southeastward before retreating as a warm front with increasing surface winds advecting a warm, moist air mass throughout the day. Although, eastern SD was in the cold sector, relatively moist conditions were already in place with Sioux Falls (FSD), Mitchell (MHE), and Watertown (ATY) all reporting dewpoints of 18° C. Pooled to the south of a stationary outflow boundary stretching from eastern NE into central IA, the most unstable air mass with surface dewpoints of 21-24° C was located in southeast NE.
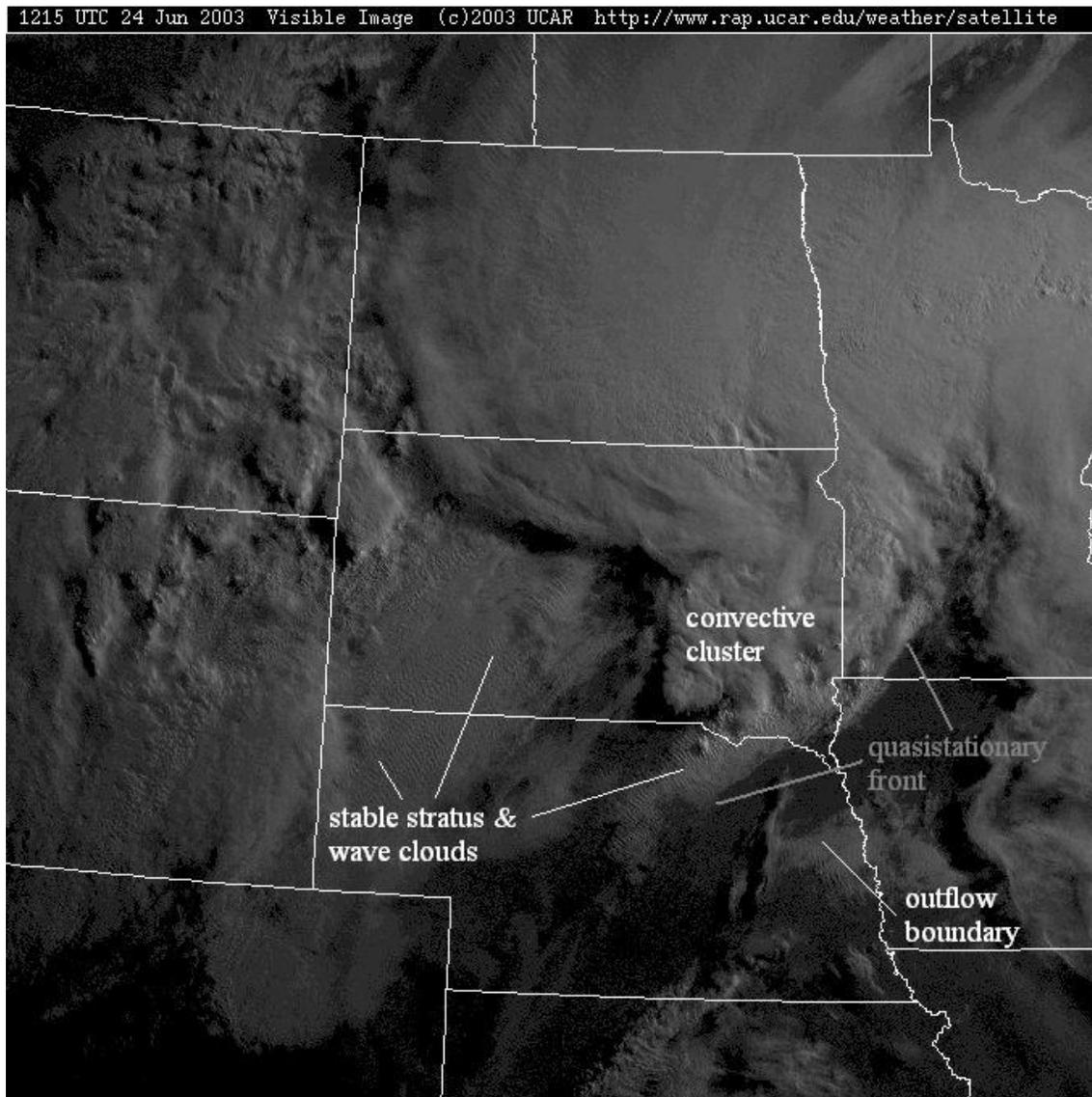
Figure 4. Visible satellite image from 1215 UTC 24 June 2003 exhibits an extensive cirrus canopy over the eastern Dakotas and MN from the convective complex associated with the shortwave moving through the region. Locations of the quasistationary front and stationary outflow boundary are denoted. [From UCAR 2003]

Visible satellite imagery at 1215 UTC (Fig. 3) depicted mostly clear skies south of the synoptic front with stratus and stable wave-like "billow" clouds along and just to the north of the boundary. A cluster of storms and anvil debris covered the eastern third of SD into MN. In the wake of the departing short wave trough, a band of clear skies stretched northward along the Missouri River in SD demarcating warmer temperatures from 18-21° C to the east, from cooler 11-17° C temperatures in the western portion of the state. With sufficient diurnal heating, the stratus cloud cover immediately to the north of the front was expected to dissipate and allow for further retreat of the warm front and outflow boundaries with persistent advection of the warm, moist air mass from the south.

With the southerly and southwesterly moist surface flow increasing to 8 to 10 m s^{-1}, the stationary front had begun retreating as a warm front by 1800 UTC (not shown). The warm front was situated from near Yankton (YKN), SD westward along the border of SD and NE to the Missouri River and southwestward to the low pressure center now over southwest NE. A cold front extended south of the low and low pressure was continuing to develop northeastward along
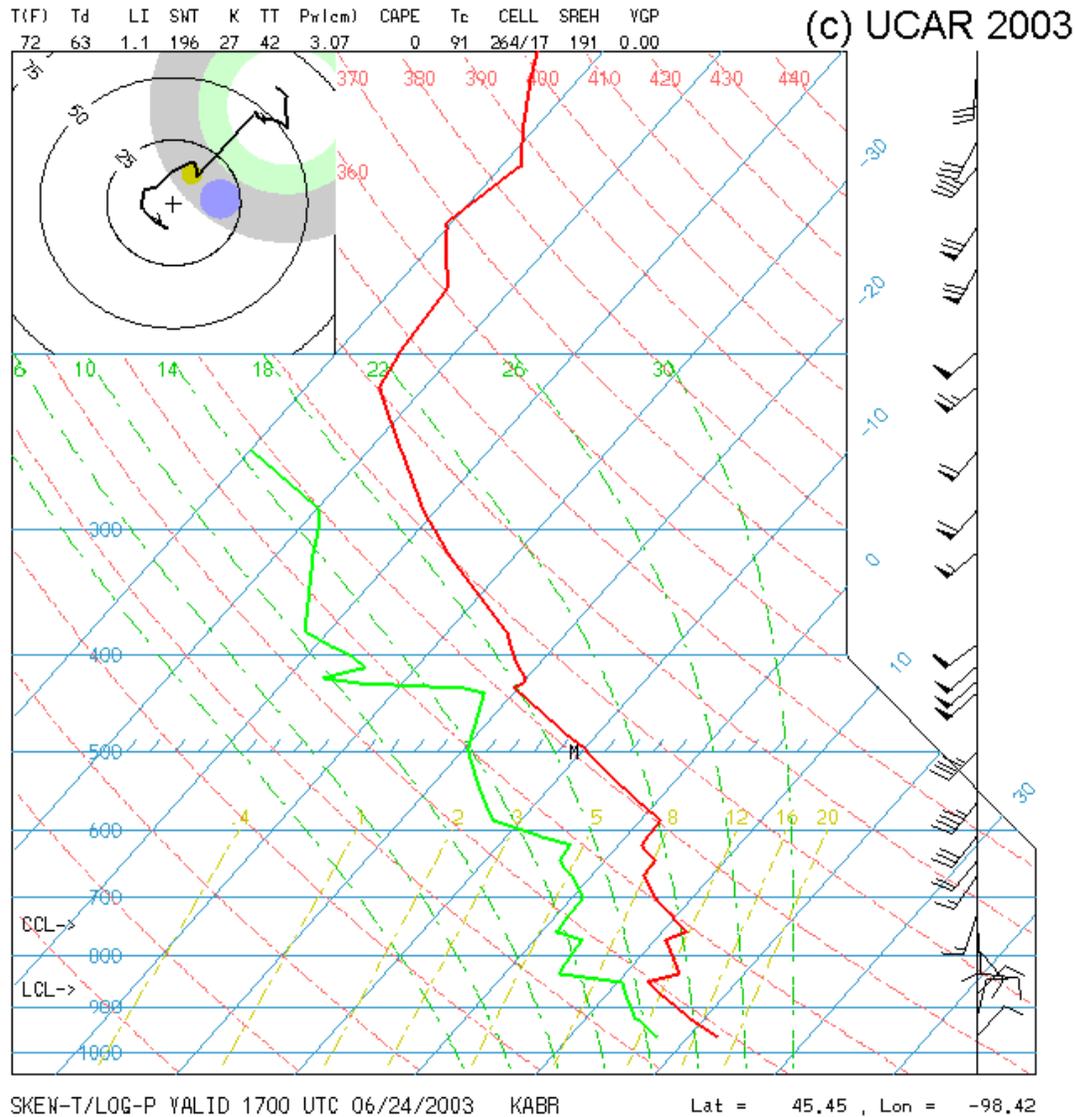
this baroclinic boundary.

Figure 5. Skew-T/log-P sounding and hodograph from 1700 UTC 24 June 2003 shows the temperature (red line)/dewpoint (green line) and wind profile from the Aberdeen (ABR) site. Temperature and dewpoint are recorded in Celsius and winds in knots. [From UCAR 2003]

An evaluation of the 1700-1800 UTC soundings from Aberdeen (ABR) and Omaha (OAX) revealed the character of the air masses north and south of the boundary. The 1700 UTC sounding from ABR (Fig. 5) showed a relatively deep moist layer from the surface to 850 mb with a surface dewpoint of $17°$ C and a mean level mixing ratio of 11.8 g kg^{-1} at that time. Layers of subsidence warming evident from 450 to 850 mb contributed to a relatively strong cap and a surface based CAPE (SBCAPE) value of only 166 J Kg^{-1} was realized. Without significant boundary layer moistening, only elevated convection was expected. The hodograph exhibited clockwise curvature in the lowest 1-km, a storm relative environmental helicity (SREH) of 191 m^2 s^{-2}, and southwesterly flow of 24.2 m s^{-1} at 500 mb. Midlevel winds of this magnitude were important for storm-scale rotation as suggested by Klemp and Rotunno (1983) and Davies-Jones and Brooks (1993). Rasmussen and Blanchard (1998) and Ramussen (2003) found that storm relative helicity in the 0-1-km boundary layer was an important parameter for distinguishing between

tornadic and nontornadic supercells.

In comparison, the 1800 UTC sounding from OAX (not shown) displayed a more uniform deep moisture layer extending from the surface to 850 mb with a surface dewpoint of 24° C and mean level mixing ratio of 18.0 g kg^{-1}. With these very moist conditions, instability parameters showed very strong instability with a SBCAPE value of 3277 J Kg^{-1}, lifted index (LI) of -7.7, and convective inhibition (CIN) of only -8.6 J Kg^{-1}. The wind shear profile showed moderate veering of the winds in the lowest 1-km of the atmosphere and the midlevel flow of 19.6 m s^{-1} was sufficient for supercells. With the advection of the warm, moist air mass pooling to the south of the synoptic boundary and destabilization ahead of the upper/mid level trough entering the Northern Plains, instability in this magnitude was expected to spread northward through southeast SD by evening. Coupled with the high instability, an easterly component to the surface winds along the warm front and outflow boundaries and an increase in the LLJ, the low level shear would be supportive of tornadoes.
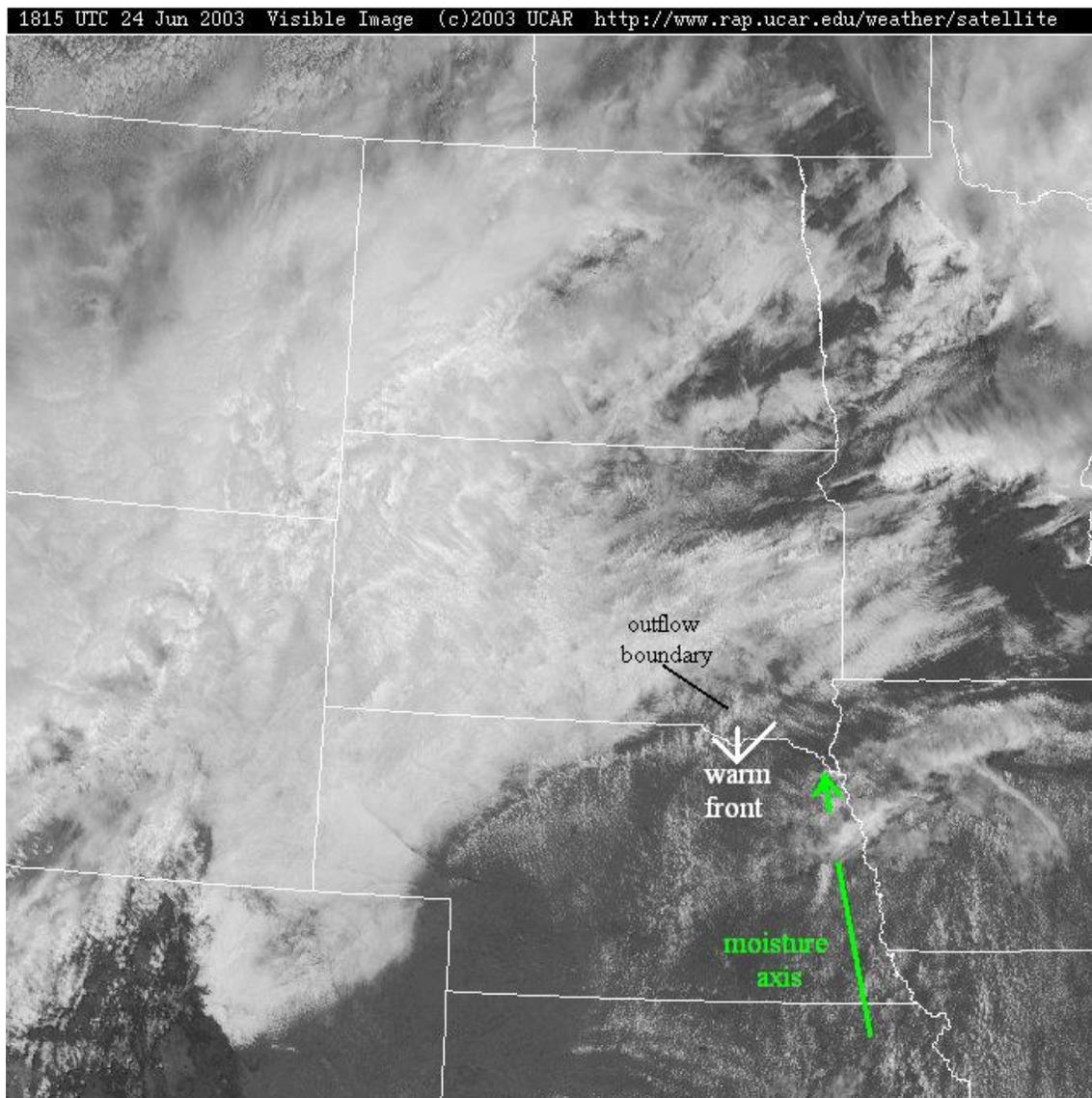

Figure 6. Visible satellite image from 1815 UTC 24 June 2003 shows an enhanced area of cumulus development at the intersection of the warm front and outflow boundary in SD. An extensive field of cumulus and stratocumulus is located south of the front. [From UCAR 2003].

3.1 Mesoanalysis

At 1815 UTC (Fig. 6), satellite imagery showed cumulus and stratocumulus developing in the warm sector. At the point of intersection of an WSW-ENE aligned outflow boundary now evident near the Missouri River in SD and the warm front along the NE/SD border, bright enhanced cumulus was developing. In between these two boundaries, mixing in the boundary layer and evapotranspiration effects resulted in dewpoints climbing to 19° C in FSD and MHE.

The most significant 3-hour pressure changes were located to the east of the Missouri River in southeast SD with Huron (HON) and Pierre (PIR) reporting -1.8 mb and MHE and Brookings (BKX) reporting -2.4 mb. These pressure falls were consistent with the passage of the retreating outflow boundary northwestward and the movement of the upper and mid level jets into the western periphery of the region.
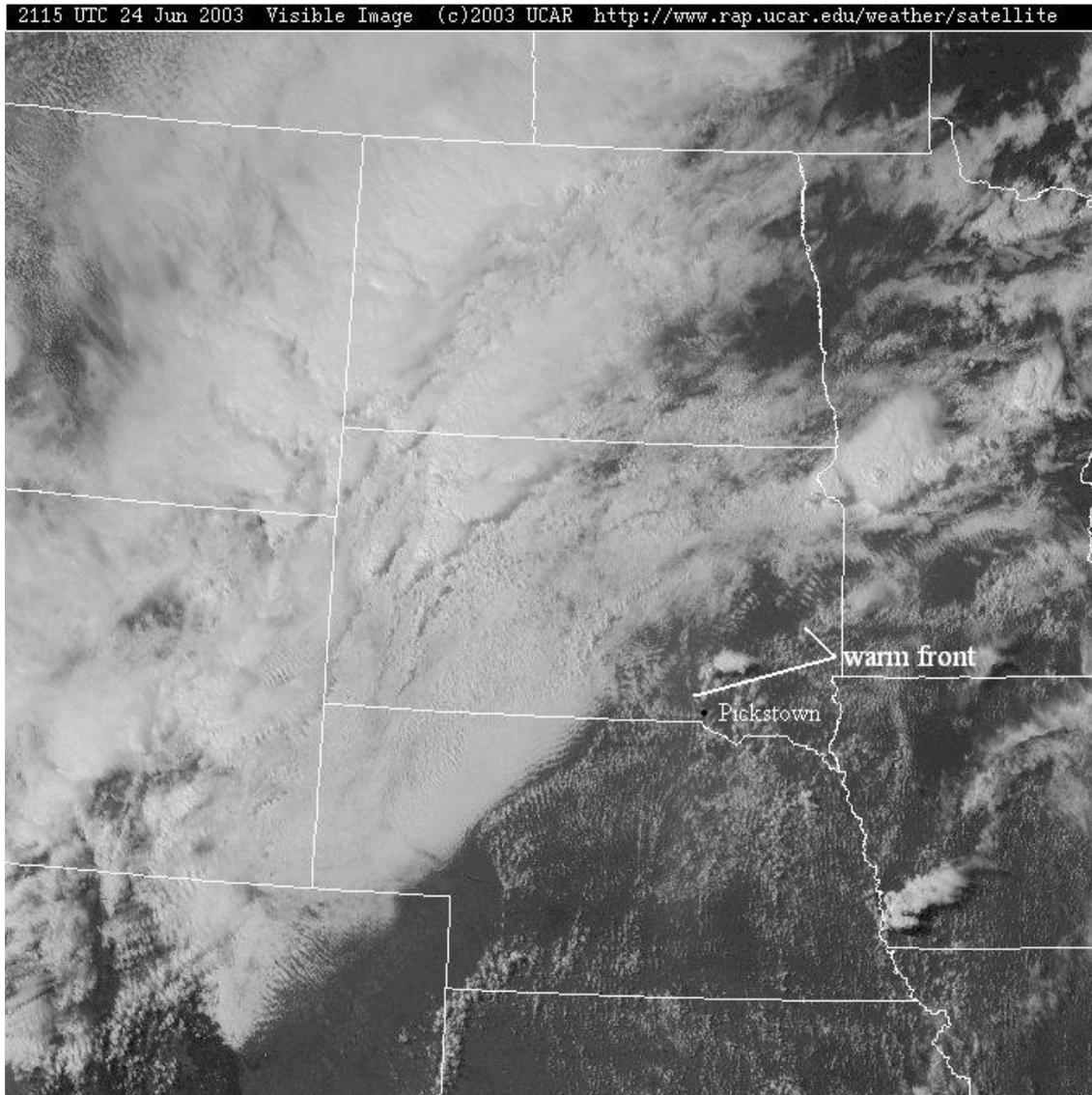

Figure 7. Visible satellite image from 2115 UTC 24 June 2003 shows the convection, with developing anvil north of Pickstown, forming along the warm front/retreating outflow boundary. [From UCAR 2003]

Satellite imagery at 2115 UTC (Fig. 7) showed a well-developed cumulus field south of the aforementioned outflow boundary which was evolving into the warm front. Along the moisture axis, towering cumuli were forming in eastern NE and near Pickstown, SD. The convection near

Pickstown quickly intensified into a supercell. This supercell moved north-northeast into the Mt. Vernon area producing two tornadoes between 2212-2235 UTC in association with the cyclic descent of the echo tops. Shortly thereafter, the supercell quickly lost strength. Fujita (1973), Lemon and Burgess (1976), and Burgess et al. (1977) documented tornadogenesis at approximately the same time as the collapse of overshooting tops. The descending echo tops were related to weakening updrafts.

At 2245 UTC (not shown), while the Mt. Vernon supercell was dissipating, a new convective tower developed to the northwest of MHE along the warm front. As the storm tracked northeastward along the boundary, it experienced an enhancement of convergence and the streamwise component of horizontal vorticity. Rasmussen et al (1998) found that outflow boundaries were rich in horizontal vorticity and were important for F2+ tornadoes. Markowski et al. (1998) found that during VORTEX almost 70% of significant tornadoes were associated with low-level boundaries. Satellite imagery showed the storm was isolated with clear skies to the west preventing detrimental anvil seeding, which was important for supercell maintenance as suggested by Rasmussen and Straka (1998). In addition, mostly clear skies to the south and southeast allowed for additional insulation and the unabated ingestion of the moist air mass.

Figure 8. At 2322 UTC 24 June 2003, as the HITPR research team is heading east on Hwy. 34 towards Woonsocket, the RFD occluding the mesocyclone is evidenced by visible observations of the clear slot. Although tornado's condensation funnel does not extend to surface, debris on the ground is observed. [Video capture by Carl R. Young].

By 2302 UTC, the storm rapidly matured to a supercell in the favorable unstable and highly sheared environment. The storm developed a strong, relatively precipitation-free rear flank downdraft (RFD) as evidenced by observation of the clear slot (Fig. 8). The visual signature of the mesocyclone being occluded by the RFD was shortly followed by a F3 tornado to the west of Woonsocket between 2316-2336 UTC (Fig. 9). Lemon and Doswell (1979), Rasmussen et al (1982), and Jensen et al (1983) observed clear slots prior to and during tornadogenesis. RFD interactions with the parent supercell were important for tornadogenesis in previous research as suggested by Ludlam (1963), Fujita (1975), Burgess et al (1977), Barnes (1978), Lemon and Doswell (1979), Brandes (1981), and Davies-Jones (1982a,b).

Figure 9. At 2332 UTC 24 June 2003, the Woonsocket tornado is losing its vertical alignment and begins to dissipate. [Video capture by Carl R. Young]

As the parent supercell of the Woonsocket tornado (hereafter referred to as the Woonsocket supercell) moved northeastward into Beadle County, it began to merge at 2347 UTC with a smaller organizing supercell moving northward from Sanborn County. Ray et al. (1976) documented vigorous intensification and eventual tornado production after a cell merger. During the cell merger process, the larger Woonsocket supercell absorbed the smaller cell and a new updraft formed in this location. Hence, the Woonsocket supercell's original mesocyclone collapsed only to reform slightly further to the east. According to Westcott (1984), a cell merger resulted in updraft intensification by reducing dry air entrainment, increasing surface convergence, and enhancing of instability by modification of the

storm-scale thermodynamic environment. As the new mesocyclone matured and intensified, there were a few brief and intermittent tornado touchdowns occurring around 2359 UTC and another at 0014 UTC 25 June 2003.
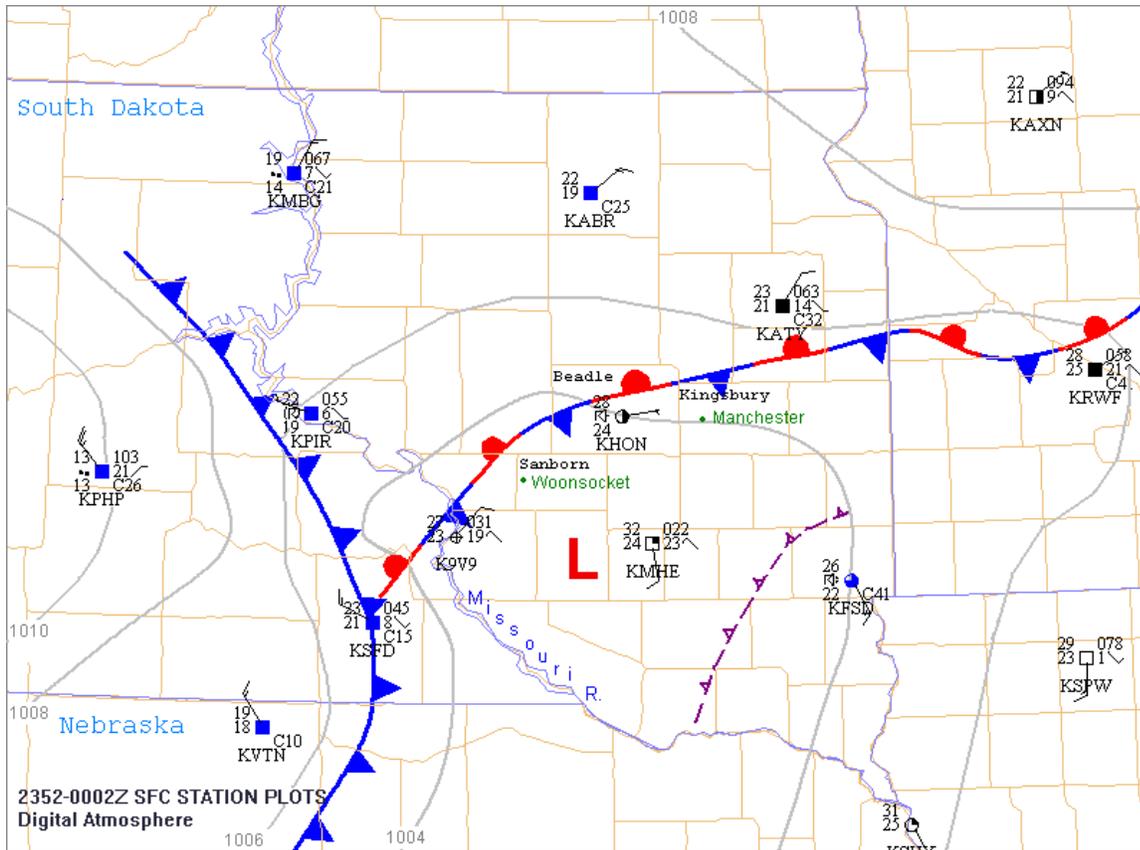

Figure 10. Surface analysis at 0000 UTC 25 June 2003 denotes frontal positions, isobars (contoured every 2 mb), and station data as Fig. 3. Select counties (Sanborn, Beadle, and Kingsbury) are labeled in the upper left-hand corner of county outlines. Select cities (Woonsocket and Manchester) are labeled in green. Active outflow boundary produced by convective activity in southeast SD is indicated by the dashed line. [Analysis created using Weathergraphics Digital Atmosphere 2004]

By 0000 UTC 25 June 2003, a quasistationary frontal boundary was in close proximity to HON and Manchester (Fig. 10). Low pressure of approximately 1002 mb had developed along this baroclinic zone and was contributing to backed surface wind flow across southeast SD thereby enhancing low level storm relative helicity. Meanwhile, extensive convection in southeast SD produced and continued to reinforce an outflow boundary propagating northwestward, but was not expected to reach the HON and Manchester area for several hours. With MHE reporting a temperature/dewpoint reading of 32/24° C, the Woonsocket supercell was continuing to ingest a warm, moist inflow into its updraft.
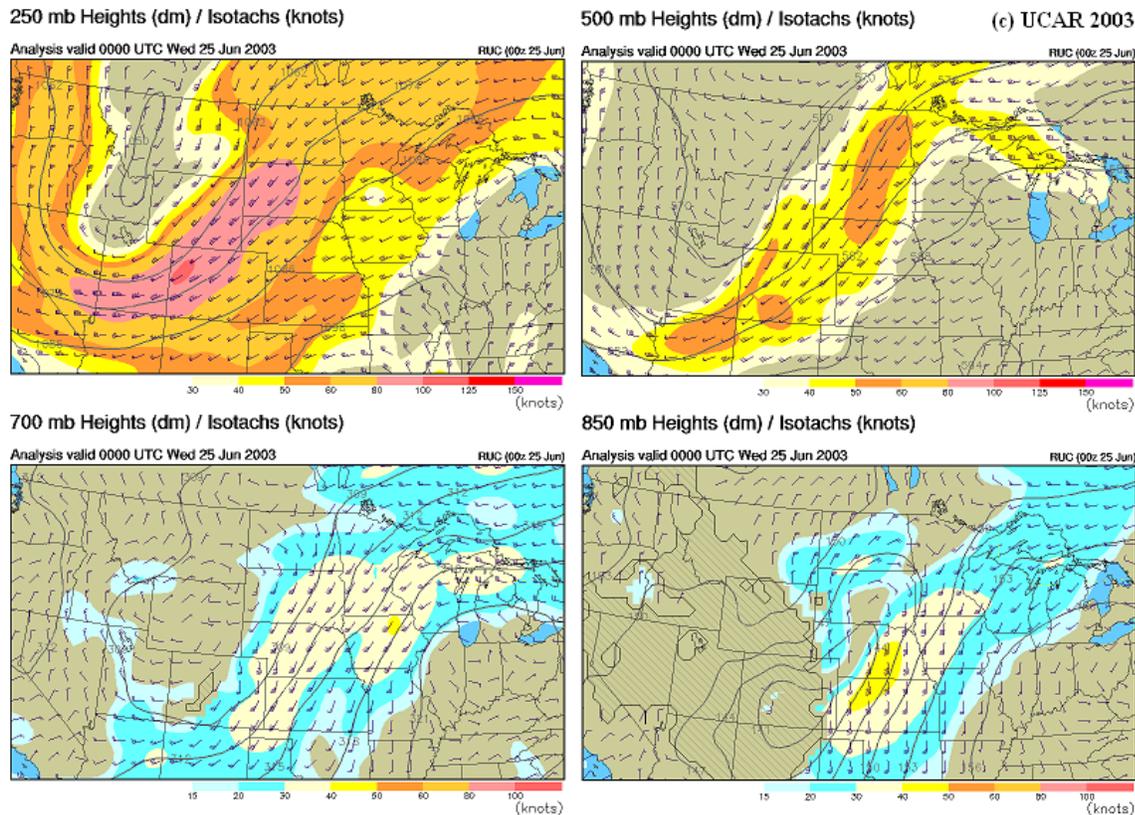
Figure 11. RUC upper air analysis 4-panel display from 0000 UTC 25 June 2003 shows the 250, 500, 700, and 850 mb heights (dm) and isotachs (wind speeds in knots and color-coded based upon scale at bottom of each diagram). [From UCAR 2003]

In addition, the wind profile was exhibiting good speed and directional shear favorable for tornadoes near HON and Manchester. Evaluating gridded 20-km Rapid Update Cycle (RUC20) numerical output analysis (Fig. 11), the 250 mb jet was positioned west of the Missouri River providing of 40-45 m s^{-1} southwesterly winds over the HON area. In phase with the upper level flow, the 500 mb southwesterly flow of 23-25 m s^{-1} was also co-located over the same region. Continued directional shear was exhibited at 700 mb with southerly winds of 20-22 m s^{-1}. As a result of a strengthening LLJ, the south-southeasterly 850 mb winds were 12-13 m s^{-1}. In the vicinity of the quasistationary front, winds were backed with southeasterly to easterly winds at 5-8 m s^{-1}. This deep layer shear contributed to 0-1-km storm relative helicity (SRH) values of 210-230 m^2 s^{-2} and 0-3-km SRH of 360-390 m^2 s^{-2} along the quasistationary frontal boundary near HON and Manchester at 0000 UTC. The mean 0-3-km SRH for tornado producing supercells was 180 m^2 s^{-2} with a 90th percentile of 411 m^2 s^{-2} according to Rasmussen and Blanchard (1998).

The Woonsocket supercell's new mesocyclone continued to intensify, especially at low levels, with large wall cloud circulation evident at its base at 0020 UTC. A few minutes later, a brief F0 tornado touched down just north of Esmond (approximately 15 km SWW of Manchester) and then reformed shortly thereafter with broader circulation at the surface. By 0029 UTC, the supercell displayed a bounded weak echo region (BWER) signature on Doppler radar (not shown) and the tornado had begun to expand rapidly to over one half-km wide at its base moving north-northwestward. At approximately 0043 UTC, the large wedge tornado made a more northward migration into the town of Manchester causing F4 damage (as concluded by Sioux Falls National Weather Service surveys following the event) and then contracted into an elephant trunk shape (Fig. 12). In the Manchester tornado's final dissipation stage, it morphed into a translucent rope structure at 0053 UTC (Fig. 13).

Figure 12. At 0050 UTC 25 June 2003, after moving northward out of Manchester, the tornado exhibits an elephant trunk structure. [Video capture by Carl R. Young]

Figure 13. At 0053 UTC 25 June 2003, the Manchester tornado exhibits a rope-like shape before the condensation funnel disappears. Debris circulation on the ground is observed for several minutes later. [Video capture by Carl R. Young]

Without any soundings in very close proximity to Manchester at that time (ABR was approximately 140 km away and north of the warm front at 0000 UTC) estimates were made of the mesoscale environment in place at the time of Manchester tornado. Although the 0000 UTC ABR sounding did satisfy the "proximity" sounding definition proposed by Brooks et al. (1999) in that the tornado occurred less than 160 km away and within one hour of the sounding, the disparity in moisture and temperature variables and winds at the surface between the two different locales resulted in the 0000 UTC ABR sounding not being truly representative of the Manchester environment. Thompson et al. (2003) found that proximity soundings from the 40-km RUC-2 forecast and analysis system were reasonably accurate in comparison to observed soundings in supercell environments and various thermodynamic and wind shear parameters derived from these RUC-2 proximity soundings were useful in discriminating between significantly tornadic (F2+), weakly tornadic (F0 to F1), and

nontornadic supercells. Although the 40-km RUC-2 was replaced by the 20-km RUC20, preliminary operational research by the Storm Prediction Center forecasters showed the research findings were still applicable. By using the RUC20 gridded 1-h forecasts (not shown) prepared at 0000 UTC 25 June, a variety of numerically modeled thermodynamic and wind shear parameters in the Manchester area were compared with the spectrum of values for significantly tornadic supercells from the Thompson et al. (2003) research. Mean level LCL (MLLCL) and 0-1 km SRH were found to be the most useful measurements for differentiating between significantly tornadic and nontornadic supercells. The Estimates for and mean level LCL (MLLCL) was 800 m and 0-1-km SRH was 240 m^2 s^{-2} in Manchester between 0000 and 0100 UTC. These values were in the upper percentiles of favorable conditions for significant tornadoes (upper 20-25 % for both 0-1-km SRH and MLLCL).   The estimate for mean 0-3-km SRH was 380 m^2 s^{-2} which was close to the 90th percentile of 396 m^2 s^{-2}.   Meanwhile, an estimate of 3600 J Kg^{-1}

MLCAPE was also close to the 90th percentile of 3683 J Kg^{-1}. LCL's less than 800 m AGL were found to be excellent discriminator between tornado-producing supercells and nontornadic supercells (generally above 1200 m) according to Rasmussen and Blanchard (1998). Thus, conditions as estimated by the RUC20 were favorable for F2+ tornadoes and as many of these parameters were in the upper percentiles, the mesoscale environment was supportive of the violent Manchester tornado

4.   DEPLOYMENT OF INSTRUMENTS

Three HITPR probes were deployed near Manchester by a chase vehicle containing all the probes. The vehicle was driven by T. Samaras and two accompanying vehicles completed the deployment team. To place the probes in the projected tornado path, the tornado movement was monitored continuously as a rapid itinerary choices were made to position the chase vehicle a safe distance in front of the tornado. The resulting trajectory is shown in Figure 14. Manchester was approached from the west on Highway 14. 425th Avenue was then taken in the north direction as the tornado approached from the south. A first probe (probe 3) was deployed about 3.21 km north of Manchester, on 206th Street, just east of 425th Avenue. A second (probe 5) and third probe (probe 6) were deployed as chase team moved northward along 425th Avenue. The deployment team then observed the progression of the tornado from north viewing point.
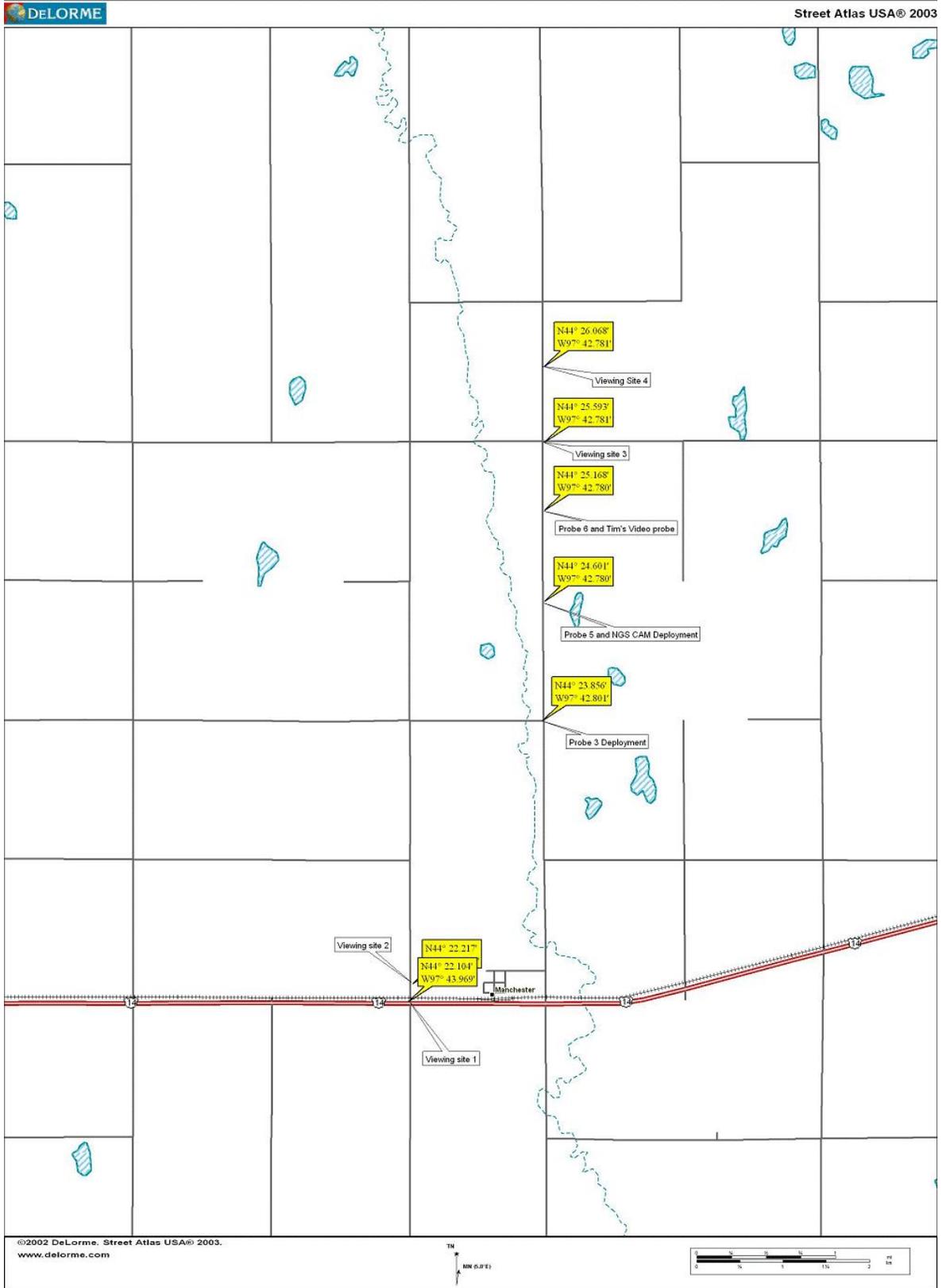
Figure 14. Map showing key locations during deployment of HITPR probes (Delorme 2003).

The deployment team first witnessed the passage of the tornado through the town of Manchester. The tornado then proceeded to pass directly over probe 3 (Figure 15).

Figure 15. Tornado at 00:45:42 UTC, 70 seconds before passing over probe 3.

The tornado continued slightly northeast, away from 425th Avenue, but then returned west to pass over probe 5 (Figure 16). The tornado then continued northwest passing more than ~100 m west of probe 6, and dissipated. The entire path of the tornado is shown in Figure 17.

Figure 16. Tornado at 00:50:17 UTC, 15 seconds after passing over probe 5.

Figure 17. Path of the Manchester tornado looking north of town. The debris path is indicated with a purple line. (Courtesy of NWS, Sioux Falls, S.D.)

5. RESULTS

The present analysis will only discuss the measurements obtained from probe 3. The measurements from probe 5 and probe 6 are left for a future discussion. Probe 3 was activated at 00:45:32 UTC, and recorded data for 33 minutes and 8 seconds.

5.1 Temperature and Humidity

The temperature was observed to steadily decrease, as the tornado passed over the probe between 70-110 seconds from probe activation (Figure 18). Because the probe was stored inside the chase vehicle prior to being deployed, the initial temperature reflected the vehicle cabin temperature. After deployment, the temperature gauge gradually reached equilibrium with outside air temperature as the wind caused air to pass through probe ports. The equilibration time of the temperature gauge is not known. This time depends mainly on the wind speed as well as the difference in temperature between the air outside and inside the chase vehicle. Higher wind speeds are expected to shorten the equilibration time, leading to a faster response time for the gauge and more accurate temperature readings.
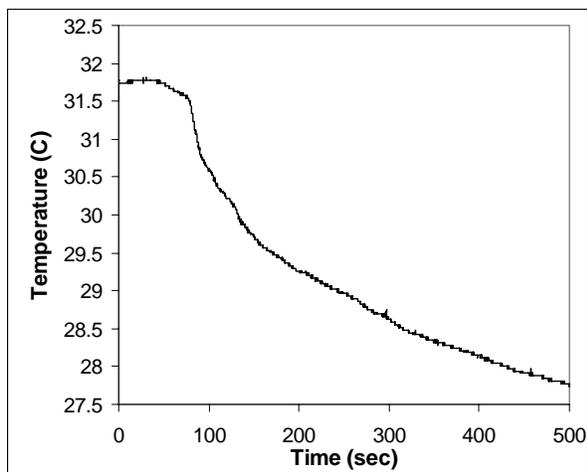

Figure 18. Temperature history from probe measurements starting at 00:45:32 UTC.

The humidity history measured by the probe is shown in Figure 19. The tornado passage occurred approximately 70-110 seconds from probe activation. The humidity gauge may be subject to the same equilibration time uncertainties as the temperature gauge.
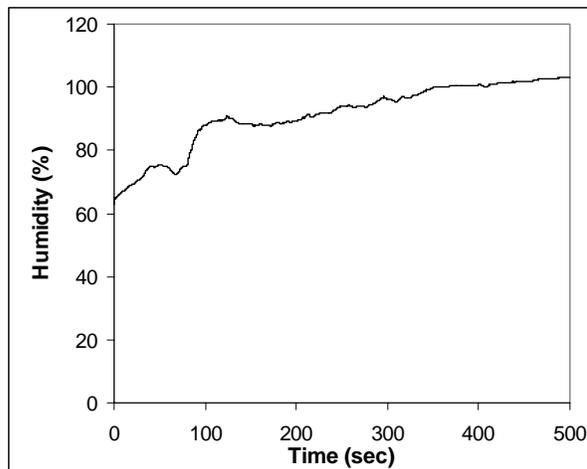

Figure 19. Humidity history from probe measurements starting at 00:45:32 UTC.

In the present analysis, the temperature and humidity measurements were used to calculate the initial air density and water vapor content.

5.2 Pressure History

The pressure history recorded by the probe is shown in Figure 21. The general macroscopic behavior of the pressure decreased as the tornado approached. The passage of the tornado core over the probe was characterized by a decrease in pressure starting at about 30 seconds, dropping more sharply at about 75 seconds, and reaching a minimum value of 850 mb at 84 seconds. This was a 100 mb drop from the initial pressure of 950 mb. The pressure then rapidly increased back up to the initial pressure in a similar fashion, forming a roughly symmetrical "V"-shaped pressure drop. Because the tornado had a translational motion, the flow field is described from a frame of reference moving with the tornado. The region in front of the tornado is referred to as upstream, and the region behind the tornado is referred to as downstream.
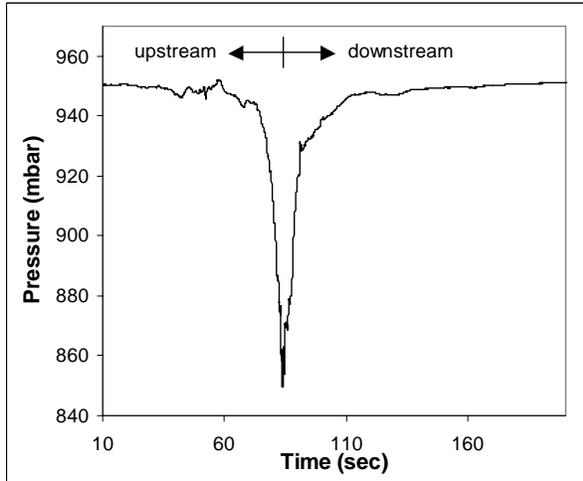
Figure 21. Pressure history from probe measurements starting at 00:45:32 UTC.

The translational speed was estimated using the time of travel between probe 3 and probe 5, and the distance between the probes. The time interval was determined using a continuous video recording of the entire deployment. Since the tornado did not travel in a straight line, the distance between the probes was estimated from maps of the area and aerial photographs of the tornado path. The translational speed was thus found to be 9.3 m/s between probe 3 and probe 5.

5.3   Probe Position Relative to Tornado Axis

Given the strong radial pressure gradient in the core region of the tornado, it is important to determine the position of the probe relative the tornado axis. A first estimate was made by inspecting the video recordings of the passage of the tornado over the probe. The position of the probe was identified on the video images using reference markers such as the road. In the video recording, the tornado appeared exactly centered over the probe position.

Further evidence of the central location of the probe relative to the tornado path was found in post-deployment measurements of the distance perpendicular to the tornado translation from the probe to the edge of the debris path. The probe was found to be equidistant from both edges of the debris path within an uncertainty of ±6 m.

Finally, calculations of the condensation funnel diameter were also found to support the passage of the tornado axis over the probe. The funnel diameter was estimated by assuming an adiabatic cooling process as the moist air outside the tornado was drawn into the core:

$$T = T_0 \left(\frac{P_0}{P} \right)^{\frac{1-\gamma}{\gamma}} \tag{1}$$

where T_0 and P_0 are the air temperature and pressure outside the tornado and γ is the ratio of specific heats. As the pressure decreases with decreasing radial distance from the tornado axis, so too does the vapor pressure of water as given by the Antoine equation:

$$\log_{10} P_\sigma = A - \left(\frac{B}{T + C} \right) \tag{2}$$

where P_σ is the vapor pressure in bar, T is the temperature in Kelvin, and A, B, C are constants equal to 5.40221, 1838.675, and −31.737 respectively for the range of temperature from 273-303 K. The dynamic humidity is given as the ratio of the partial pressure of water in the air to the vapor pressure. As the pressure and temperature decreased towards the tornado axis, the dynamic humidity increased. The dynamic humidity is shown as a function of the distance traveled by the tornado (Figure 22). This distance was calculated using the translational speed of the tornado of 9.3 m/s. Condensation was assumed to occur when saturation reached 100% humidity, resulting in a visible cylindrical condensation region about the minimum pressure point (shown by the dashed red lines in Figure 22). The diameter of this region was found to be 48 m. This value is expected to be an upper bound since it is calculated assuming instantaneous equilibration of the fluid states when the saturation point is reached. There have been studies suggesting that the condensation process in tornadoes is a non-equilibrium process (Jischke and Parang 1975). This would delay the condensation, resulting in a smaller condensation cylinder.
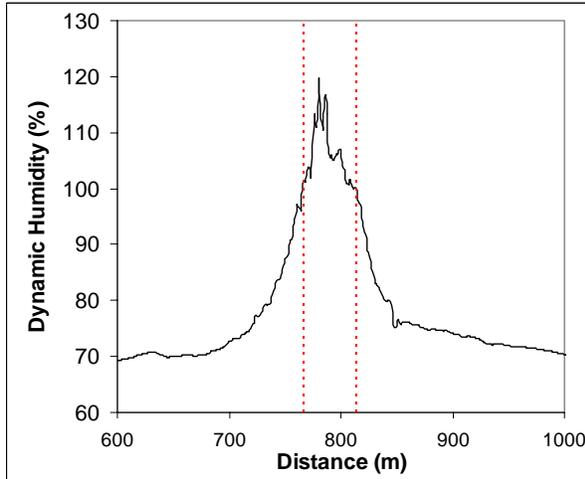
Figure 22. Dynamic humidity as the tornado passed over the probe.

The calculated funnel condensation diameter of 48 m agreed well with the funnel diameter of 37 m ±10 m estimated from inspection of the video images. If the tornado core axis had not passed directly over the probe, the magnitude of the peak pressure drop would have been reduced, and the calculated funnel diameter would have been smaller than the observed diameter. If the tornado axis had passed far from the probe, the pressure drop would not have been sufficient to cause condensation. The agreement between the calculated and measured diameters in the present case suggests that the tornado axis had passed very close to the probe.

5.4 Maximum Velocity Estimates

A simple estimate of the maximum tangential velocity (v_{max}) in the tornado can be made by applying the cyclostrophic balance equation:

$$\frac{\rho v^2}{r} = \frac{\partial p}{\partial r} \tag{3}$$

where ρ is the density, p is the pressure, v is the tangential flow, and r is the radius, to a simple Rankine vortex model, giving the expression for the maximum velocity (Lewellen 1976):

$$v_{max} = \left(\frac{\Delta p}{\rho} \right)^{1/2} \tag{4}$$

where Δp is the pressure drop. Using this relation, v_{max} is found to be 98 m/s. Cyclostrophic balance, however, applies more to the core flow region in the upper levels of the tornado vortex, and is usually not valid in the corner region which is strongly influenced by ground effects. Furthermore, maximum velocities have been found to occur in the corner region rather than in the upper core in three-dimensional simulations of tornadoes (Lewellen and Lewellen 1997). Hence this simplified estimate should be interpreted with care.

Another method of estimating the maximum tangential velocity is to apply the cyclostrophic balance equation directly to the pressure trace (Figure 21). The pressure variation with time is converted to a dependence on distance using the translational speed of the tornado. The origin of the tornado vortex is then chosen as the point where the minimum pressure is reached. The resulting pressure dependence on radial distance is differentiated and converted to velocity using equation 3. The resulting tangential wind speed is shown in Figure 23. Due to signal noise and small-scale pressure fluctuations, a moving average method was used to filter the trace before differentiating it. The results using two window sizes are shown in Figure 23. Window sizes of 10 m and 20 m correspond to time-averaging the signal over one and two seconds respectively. The maximum speed was found to be 92 m/s. This speed is in the upper range of an F-3 tornado, supporting visual observations that the tornado was weakening from its F-4 state in Manchester (**Figure 12**, **Figure 13**). A core radius "a" of 45 m is found, as defined by the distance between the velocity maxima on either side of the axis. The core is also found to be asymmetrical about the axis, with a lower peak velocity and slightly shorter core radius on the upstream side. This may be due to the translation motion of the tornado.
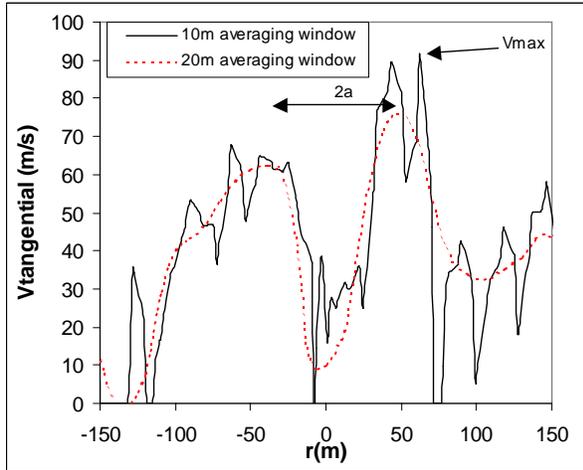
Figure 23. Tangential wind speed calculated from cyclostrophic balance.

Although the cyclostrophic balance is generally not valid close to the ground, using it to estimate maximum wind speed may be reasonable in certain cases. When applying the cyclostrophic balance to ground-based measurements inaccuracies occur due to strong vertical pressure gradients. However, laboratory simulations of vortices have shown that strong vertical gradients mainly occur in vortices with swirl ratios between about 0.2 and 0.6 (Church and Snow 1984, Pauley 1989). This is supported by numerical simulations that show weak pressure gradients in high-swirl ratio vortices (Lewellen and Lewellen 1997). Hence if the Manchester tornado vortex could be characterized by a swirl ratio outside of the problematic range between 0.2 and 0.6, the above estimates of wind speed could be acceptable.

Additional support to the validity of applying cyclostrophic balance to ground-based pressure measurements can also be found in comparisons between wind speeds calculated in this manner and wind speeds measured by Doppler radar. Wurman and Samaras (2004) found reasonable agreement between the two.

5.5 Vortex Model Comparisons

Using a v_{max} of 92 m/s and a core radius of 45 m obtained from cyclostrophic balance calculations, the pressure drop was calculated in a simple Rankine vortex (Winn et. al. 1999). The

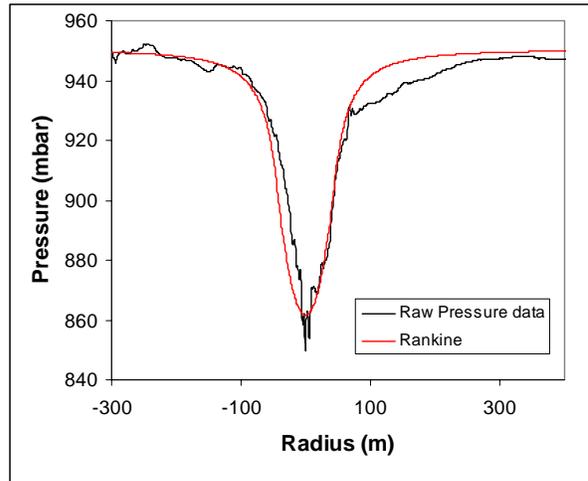results show reasonably good agreement between the model and measurements (Figure 24).

Figure 24. Comparison between a Rankine vortex and tornado pressure measurements.

Further comparisons were made with a more realistic Burgers-Rott vortex (Winn et. al. 1999), which does not have a discontinuity at the tangential velocity maximum and incorporates a central updraft core. The pressure $p(r,z)$ in the Burgers-Rott vortex is given by:

$$p(r,z) = p(0,0) + \rho \int_0^r \frac{v_\phi^2}{r} dr - \frac{\rho b^2}{2}\left(r^2 + 4z^2\right)$$

(5)

where z is the axial distance, v_ϕ is the tangential velocity, and b is a constant. This model captures the global characteristics of a single-cell vortex. The following values were used in applying the model:

- axial pressure at the ground: 858 mb
- circulation: 2.6 x 10^6 m^2/s
- eddy viscosity: 10 m^2/s
- b:1.5 x 10^{-2} s^{-1}

The value of b was adjusted to obtain the best fit between the model pressure and the measured data: The agreement between the two is slightly improved over the Rankine model comparison (Figure 25).
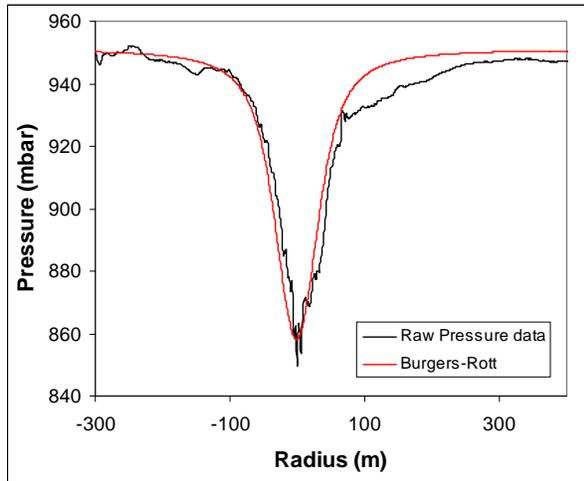
Figure 25. Comparison between a Burgers-Rott vortex and tornado pressure measurements.

In comparisons between the vortex models and the measured pressure, the good agreement suggests that the measured pressure may be close to those in the upper core region of the tornado, i.e. vertical pressure gradients may be weak. The agreement also suggests that the global tornado structure may be of a single-cell vortex type.

Discrepancies were also observed between the models and measurements. In the upstream measured pressure between –300 m and –100 m, we note large scale pressure fluctuations with length-scales on the order of a few tens of meters. These fluctuations may be due to instabilities in the boundary layer causing separation and reattachment. These fluctuations are absent in the downstream portion of the tornado. This may be due to the higher Reynolds number downstream caused by tornado translation. A higher Reynolds number could lead to smaller-scale turbulence, and thus smaller pressure fluctuations downstream. An interesting feature is the sharp kink and abrupt change in slope on the downstream pressure at about 65 m from the axis. This pressure behavior resembles a transition point with turbulent wake features downstream of the kink. Finally, we note that the measured pressure trace is slightly shifted downstream compared to the model curve. This asymmetry may be due to the translational motion of the tornado.

6. SUMMARY AND FUTURE WORK

A HITPR measurement probe was deployed in the path of a weakening F-4 tornado near Manchester on June 24th, 2003. Condensation funnel calculations combined with visual observations suggest that the tornado axis passed very near the probe, providing near-maximal pressure drop measurements. Cyclostrophic balance calculations provided reasonable maximum wind speed and core diameter results, indicating that the ground-based pressure measurements provided a global estimate of behavior in the higher core flow region of the tornado. Comparisons to analytical vortex models suggest that the tornado had global characteristic similar to a single-cell vortex, and that vertical pressure gradients were weak. Fluctuations in the pressure upstream of the tornado indicate possible separation and reattachment of the boundary layer, implying a moderate Reynolds number conducive to transitional behavior. The higher downstream Reynolds number may account for an observed abrupt transition to a higher momentum transport zone similar to a turbulent wake.

Additional analysis of the pressure traces involving comparisons with simulated laboratory models may yield additional insight into the tornado structure details.

7. ACKNOWLEDGEMENTS

8. REFERENCES

Barnes, S. L., 1978: Oklahoma thunderstorms on 29-30 April 1970, Part I: Morphology of a tornadic storm. *Mon. Wea. Rev.,* **106**, 673-684.

Bluestein H.B., and Golden J.H. (1993). A review of tornado observations, *The tornado: its structure, dynamics, prediction, and hazards, Geophys. Monogr. Ser.*, C. Church, C. Burgess, C. Doswell, and R. Davies-Jones Eds. **79**.

Brandes, E. A., 1981: Fine Structure of the Del City-Edmond tornadic mesocirculation, *Mon. Wea. Rev.,* **109**, 635-647.

Brooks, H. E., C. A. Doswell III, and J. Cooper, 1994: On the environments of tornadic and nontornadic mesocyclones. *Wea. Forecasting,* **9**, 606-618.

Burgess, D. W., R. A. Brown, L. R. Lemon, and C. R. Safford, 1977: Evolution of a tornadic thunderstorm. Preprints, *10th Conf. on Severe Local Storms,* Omaha, NE, Amer. Meteor. Soc., 84-89.

Church, C.R., and Snow, J.T. (1984). Measurements of

axial pressures in tornado-like vortices, *J. Atmos. Sci.* **42:6**, pp. 576-582.

Davies-Jones, R. P., 1982a: A new look at the vorticity equation with application to tornadogenesis. Preprints. *12th Conf. on Severe Local Storms*, San Antonio, TX, Amer. Meteor. Soc., 249-252.

——, 1982b: Observational and theoretical aspects of tornadogenesis. *Intense Atmospheric Vortices*, L. Bengtsson and J. Lighthill, Eds. Springer-Verlag, 175-189.

——, and H. E. Brooks, 1993: Mesocyclogenesis from a theoretical perspective. *The Tornado: Its Structure Dynamics, Prediction, and Hazards, Geophys. Monogr.,* No. 79, Amer. Geophys. Union, 104-114.

Delorme 2003. Street Atlas USA (on compact disc).

Fujita, T. T., 1973: Proposed mechanism of tornado formation from rotating thunderstorms. Preprints, *Eighth Conf. on Severe Local Storms,* Denver, CO, Amer. Meteor. Soc., 259-266.

——, 1975: New evidence from the April 3-4 tornadoes. Preprints, *Ninth Conf. on Severe Local Storms*, Norman, OK, Amer. Meteor. Soc., 248-255.

Jensen, B., T. P. Marshall, M. A. Mabey, and E. N. Rasmussen, 1983: Storm scale structure of the Pampa storm. Preprints. *13th Conf. on Severe Local Storms,* Tulsa, OK, Amer. Meteor. Soc., 85-88.

Jischke, M.C., and Parang, M. (1975). Fluid dynamics of a tornado-like vortex flow. Final Report NOAA grant N22-200-72(G) and 04-4-022-13, University of OK.

Klemp, J. B., and R. Rotunno, 1983: A study of the tornadic region within a supercell thunderstorm. *J. Atmo. Sci.*, **40**, 359-377.

Lemon, L. R., and D. W. Burgess, 1976: Tornadic storm airflow and morphology derived from single Doppler radar measurements. The Union City, Oklahoma Tornado of 24 May 1973, R. A. Brown, Ed. NOAA Tech Memo. ERL-80, National Severe Storms Laboratory, 85-106.

——, and C. A. Doswell, 1979: Severe thunderstorm evolution and mesocyclone structure as related to tornadogenesis. *Mon. Wea. Rev.,* **107**, 1184-1197.

Lewellen, W.S. (1976). Theoretical models of the tornado vortex, *Proceedings of the Symposium on Tornadoes, Assessment of Knowledge and Implications for Man*, R. E. Peterson Ed., held in Lubbock, TX, on June 22-24.

Lewellen, W.S., and Lewellen, D.C. (1997). Large-eddy simulation of a tornado's interaction with the surface, *J. Atmos. Sci.*, **54:5**, pp. 581-605.

Lewellen, D.C., Lewellen, W.S., and Xia, J. (2000). The influence of a local swirl ratio on tornado intensification near the surface, *J. Atmos. Sci.*, **57**, pp. 527-544.

Ludlam, F. H., 1963: Severe Local Storms: A review. *Severe Local Storms, Meteor. Monogr.*, No. 27, 1-30.

Markowski, P. M., E. N. Rasmussen, and J. M. Straka, 1998: The occurrence of tornadoes in supercells interacting with boundaries during VORTEX-95. *Wea. Forecasting,* **13**, 852-859.

Pauley, R. L. (1989). Laboratory measurements of axial pressures in two-celled tornado-like vortices, *J. Atmos. Sci.* **46:21**, pp. 3392-3399.

Rasmussen, E. N., 2003: Refined Supercell and Tornado Forecast Parameters, *Wea. Forecasting,* **18**, 530-535.

——, and D. O. Blanchard, 1998: Baseline climatology of sounding-derived supercell and tornado forecast parameters. *Wea. Forecasting*, **13**, 1148-1164.

——, R. E. Peterson, J. E. Minor, and B. D. Campbell, 1982: Evolutionary characteristics and photogrammetric determination of windspeeds within the Tulia outbreak tornadoes 28 May 1980. Preprints, *12th Conf. on Severe Local Storms,* San Antonio, TX, Amer. Meteor. Soc., 301-304.

——, S. Richardson, J. M. Straka, P. M. Markowski, and D. O. Blanchard, 2000: Association of significant tornadoes with a baroclinic boundary on 2 June 1995. *Mon. Wea. Rev.,* **128**, 174-191.

——, and J. M. Straka, 1998: Variations in supercell morphology. Part I: Observations of the role of upper-level storm-relative flow. *Mon. Wea. Rev.,* **126**, 2406-2421.

Ray, P. S., B. C. Wagner, R. B. Wilhelmson, and J. B. Klemp, 1981: The morphology of several tornadic storms on 20 May 1977. *J. Atmos. Sci.,* **38**, 1643-1663.

Samaras, T.M., and Lee, J.J. 2003. Pressure measurements within a large tornado, *Proc. 84th American Meteorological Society Annual Meeting*, 11-15 January, Seattle, WA.

Samaras, T.M. 2004: An historical perspective of in-situ observations within tornado cores. *Proc. 22nd Conf. on Severe Local Storms*, Paper 11.4, Hyannis, MA.

Thompson, R. L., R. Edwards, J. A. Hart, K. L. Elmore, P. M. Markowski, 2003: Close proximity soundings within supercell environments obtained from the Rapid Update Cycle. *Wea. Forecasting,* **18**, 1243-1261.

Westcott, N., 1984: A historical perspective on cloud mergers. *Bull. Amer. Meteor. Soc.,* **65**, 219-226.

Winn, W. P., Hunyady, S.J., and Aulich, G.D. (1999). Pressure at the ground in a large tornado, *J. Geophys. Res.* **104:D18**, pp. 22067-22082.

Wurman, J. 2004. Comparison of in-situ pressure and DOW Doppler winds in a tornado. *Proc. 22nd Conf. on Severe Local Storms,* Hyannis, MA.